Influence of shear and deviatoric stress on the evolution of permeability in fractured rock

Igor Faoro,[1] Andre Niemeijer,[1,2] Chris Marone,[2] and Derek Elsworth[1]

[1]   The evolution of permeability in fractured rock as a function of effective normal stress, shear displacement, and damage remains a complex issue. In this contribution, we report on experiments in which rock surfaces were subject to direct shear under controlled pore pressure and true triaxial stress conditions while permeability was monitored continuously via flow parallel to the shear direction. Shear tests were performed in a pressure vessel under drained conditions on samples of novaculite (Arkansas) and diorite (Coso geothermal field, California). The sample pairs were sheared to 18 mm of total displacement at 5 μm/s at room temperature and at effective normal stresses on the shear plane ranging from 5 to 20 MPa. Permeability evolution was measured throughout shearing via flow of distilled water from an upstream reservoir discharging downstream of the sample at atmospheric pressure. For diorite and novaculite, initial (preshear) fracture permeability is $0.5–1 \times 10^{-14}$ m^2 and largely independent of the applied effective normal stresses. These permeabilities correspond to equivalent hydraulic apertures of $15–20$ μm. Because of the progressive formation of gouge during shear, the postshear permeability of the diorite fracture drops to a final steady value of 0.5×10^{-17} m^2. The behavior is similar in novaculite but the final permeability of 0.5×10^{-16} m^2 is obtained only at an effective normal stress of 20 MPa.

1.   Introduction

[2]   Fluid flow and transport in fracture networks in rocks are relevant to a broad variety of scientific and industrial problems and processes, and have received considerable attention [e.g., *Cook*, 1992]. Most rock masses contain complex, interconnected networks of fractures with rough boundaries and breccia or, in some cases, gouge. Because of their high transmissivity, fractures are often conduits for fluid flow and transport; and their presence is critical in the recovery of hydrocarbons and geothermal fluids, and in mediating the evolution of fault zones and hydrothermal deposits.

[3]   Rocks and soils typically contain pores and fractures with a complex distribution of sizes and shapes [*Sahimi*, 1993, 1995]. Flow and transport of fluids in such porous media occurs not only through the microscopic pores, but also through fractures, which are typically much larger than the pores. Much effort has been expended to characterize the geometry of natural fracture systems as a precursor to defining their mechanical and transport properties [*Crampin and Chastin*, 2003].

[4]   For example, the orientation and intensity of fracturing in the subsurface of fracture-controlled geothermal fields are detected by measuring the fast shear wave polarization and time delay from local micro earthquakes [*Lou and Rial*, 1997; *Vlahovic et al.*, 2003a, 2003b; *Elkibbi and Rial*, 2003, 2005; *Yang et al.*, 2005]. Also, fracture filling and fluid properties are related to fracture compliances and may be inferred from seismic data [e.g., *Liu et al.*, 2001, 2002; *Maultzsch et al.*, 2003].

[5]   Fracture apertures and fracture connectivity together control the transport properties of fractured rocks, although the former is difficult to infer either directly or indirectly from seismic data. However, it has been argued that shear wave anisotropy is sensitive to the fracture aspect ratio defined as the ratio of fracture aperture to length and therefore is related to the ambient stress field in the crust [*Crampin and Chastin*, 2003].

[6]   Moreover there have been many attempts to correlate the elastic (mechanical) and hydraulic (transport) properties of fractured rock [*Cook*, 1992; *Bayuk and Chesnokov*, 1998; *Pyrak-Nolte*, 2002; *King*, 2002; *Liu et al.*, 2004]. These correlations are not always straightforward, and can sometimes be enigmatic, with the result that the inversion of seismic data for hydraulic transport properties is complex and must be done with care [*Rasolofosaon and Zinszner*, 2002].

[1]Department of Energy and Mineral Engineering and the Energy Institute, Pennsylvania State University, University Park, Pennsylvania, USA.
[2]Department of Geosciences and the Energy Institute, Pennsylvania State University, University Park, Pennsylvania, USA.
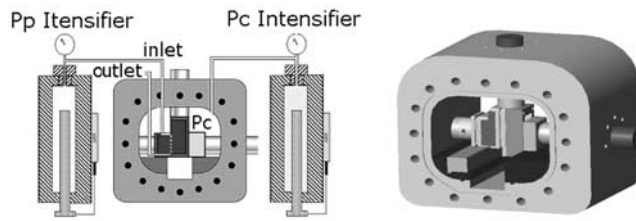
Figure 1. Equipment arrangement showing pressure vessel, pressure intensifiers, schematic of plumbing arrangement, and experiment configuration for direct shear of the fracture samples.

[7] In summary, although there has been considerable success in the seismic characterization of natural fractures, it remains difficult to quantify several fundamental factors, including fracture density, shape, aperture, and connectivity. These are important initial conditions for hydrologic models, which underscores the difficulty of evaluating the evolution of fracture properties with stress history. A key purpose of this paper is to provide direct information on the relationship between fracture properties.

[8] Recently other studies investigating the evolution of the mechanical and transport proprieties of fractured rocks relate the mechanical effects of crack formation, dilation, and closure, with chemical effects of stress mediated dissolution and precipitation. In particular, these effects are common either for micro cracks [*Tenthorey et al.*, 2003] or faults [*Tadokoro and Ando*, 2002; *Yasuhara et al.*, 2005]. The temperature and chemical potential of the circulating fluid also has a significant influence on the evolution of strength and permeability. This is apparent in observations at high temperatures in granite [*Moore et al.*, 1994], and at lower temperatures in tuff [*Lin and Daily*, 1990] and in composite aggregates of quartz [*Elias and Hajash*, 1992], halite [*Gratier*, 1993], calcite [*Zhang et al.*, 1994] and albite [*Hajash et al.*, 1998; *Siddiqi et al.*, 1997].

[9] Although reactive transport is somewhat well defined in granular aggregates [*Raj*, 1982; *Tada and Siever*, 1989] the relevant processes in fractured systems are poorly understood. For this reason, predicting changes in transport parameters due to pressure solution and the circulation of geothermal fluids remains a complex task [*Moore et al.*,1994; *Lin et al.*, 1997; *Durham et al.*, 2001; *Polak et al.*, 2003; *Yasuhara et al.*, 2004].

[10] In this study we investigated the changes in permeability of artificial fractures in novaculite and diorite under a range of conditions. In particular we focus on the effects that shear stress and triaxial stress state exert on mechanical (compaction and dilation), hydraulic (permeability) and chemical (advection and dissolution phenomena) behaviors of the fractures.

2. Experimental Method

[11] Experiments were conducted on mated smooth-faced rock samples confined under normal stress. The samples were sheared, and concurrent measurements of strength and permeability were made as a function of shear offset under isothermal conditions. We begin by documenting the capa-

bilities of the system, the experimental procedure, and key features of data analysis.

2.1. Experimental Equipment

[12] The equipment consists of a steel pressure vessel of dimensions $\sim$50 $\times$ 50 $\times$ 40 cm, capable of applying confining and pore pressures of up to 70 MPa and independent applied biaxial stresses in excess of 300 MPa. The vessel has removable doors to allow access to the sample during setup (Figure 1). In our experiments, samples are placed within this pressure vessel (Figure 2) and are loaded biaxially by servo-controlled hydraulic rams. Normal and shear stresses on the fracture surface are applied directly via loading pistons and are measured to a resolution of 0.01 MPa. Relative displacements parallel and perpendicular to the fracture plane are recorded by two DCDTs, accurate to 0.1 μm, mounted on the loading rams external to the pressure vessel. The sample assembly is jacketed within a thin, flexible latex membrane (Figure 2) and confining pressure is applied via the surrounding fluid. True triaxial loading conditions are achieved via the two loading pistons and the confining pressure, each of which is servo-controlled independently (Figure 1). In addition, two high-precision servo-controlled pressure intensifiers are used to apply pore fluid pressure to the sample.

[13] We conducted experiments on paired prismatic rock plates 11–12 mm thick, 45 mm wide and 50 and 70 mm long, respectively (Figure 2). Direct shear is accomplished by motion of the longer block relative to a stationary shorter block, with constant nominal contact area of 45 $\times$ 50 mm (Figure 2). The forcing platens have fittings and fluid delivery ports for pore fluid access to the sample. The sample assembly is first loaded in the fracture-normal direction and then subject to confining pressure and vertical load to apply shear stress on the fracture plane. A roller way bearing allows a double direct shear configuration to be used as single direct shear (Figures 1 and 2).

[14] In our experiments a load is applied at the top of the longer forcing block, producing shear relative to the static side block (Figures 1 and 2). Pore fluid is supplied along a line source at the top and base of the static load platen (Figure 2), allowing either uniform or differential fluid pressures to be applied along the shear surface. This fluid input is controlled by upstream and downstream reservoirs (Figure 1). The jacketing system has been configured to guarantee a seal on the sample during the large relative displacements sustained during these shear experiments. It comprises two layers of latex tubing (7 cm diameter and 15 cm length) surrounding the sample, sealed by two rubber O-rings constricted by two aluminum collars (54.5 $\times$ 70 mm and 54.5 $\times$ 90 mm). Between the latex layer and the surfaces of the sample another rubber layer, which is 3 mm thick, is used to protect the jackets from puncturing when a confining pressure is applied (Figure 2).

2.2. Experimental Procedure

[15] The faces of the rock plates are surface ground to be both square and parallel. The contact surfaces are then roughened by polishing with #60 grit for approximately 10 min and finally rinsed with distilled water and jacketed. Samples are positioned in the pressure vessel, then normal stress is applied and pore pressure intensifiers are
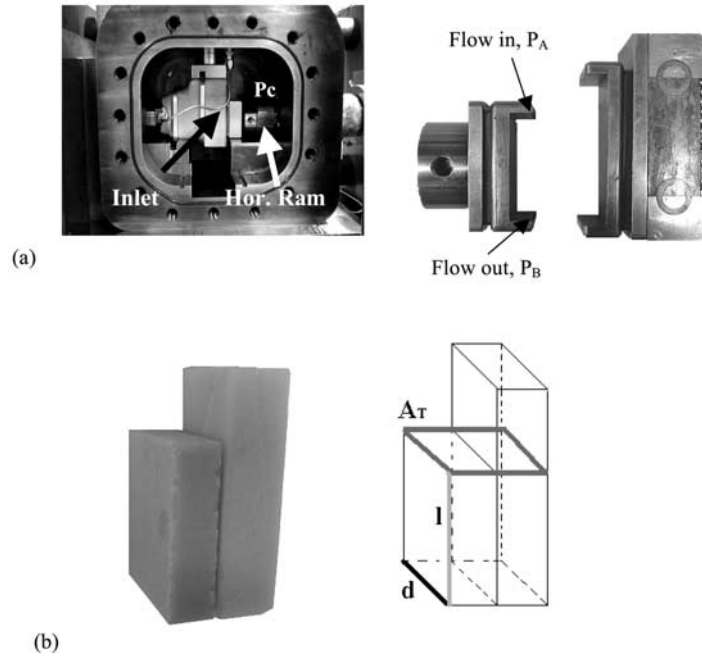
Figure 2. (a) Sample setup showing jacket, sealing collars, fluid piping internal to the pressure vessel, flow path and line source fluid distribution at top and bottom of fracture surface, access, sample holders, and roller bearing for direct shear in the double direct shear configuration. (b) Photo of novaculite sample and schematic of sample geometry showing main dimensions. A_T is the area perpendicular to the flow direction, which is used in Darcy's law.

connected, after which the vessel doors are closed and sealed. The pressure vessel is then filled with the confining fluid (XCELTHERM® 600 oil from Radco Industries). Permeability evolution is measured continuously before, during and after the shear test via flow of distilled water from an upstream reservoir that discharges downstream at atmospheric pressure. The discharge fluid is collected for chemical analysis using mass spectrometry (ICP-MS). The shear test begins after the flow rate has reached steady state.

[16] Permeability is calculated from Darcy's law according to

$$k = \frac{Q \cdot \mu \cdot l}{A_T \cdot \Delta P}, \qquad (1)$$

where k is permeability (m^2), Q is flow rate (m^3/s), μ is dynamic viscosity (Pa s), l is length of the sample (m), A_T is area perpendicular to the flow direction (see Figure 2) (m^2), and ΔP is the pore pressure drop over length l (Pa).

[17] The flow rate is calculated from

$$Q = \frac{Ppdisp}{\Delta t} \cdot A_{Pp}, \qquad (2)$$

where $Ppdisp$ is given by pore pressure intensifier displacement (m), Δt is the time interval (s), and A_{Pp} is the cross-sectional area of pore pressure intensifier piston (m^2).

[18] Furthermore, the equivalent hydraulic aperture of the artificial fracture between the two sample plates, w, is evaluated as a function of the recorded flow rate, the sample

width d, and the pressure drop measured over the sample length as (Figure 2 shows details of the geometry):

$$Q = d \cdot \frac{w^3}{12 \cdot \mu} \cdot \frac{\Delta p}{dl}. \qquad (3)$$

Two identical suites of experiments were completed on samples of diorite and novaculite. Experiments were conducted at room temperature and with a pore fluid pressure gradient Δp of 0.1 MPa. Each experiment suite included three values of effective normal stress (5, 10, and 20 MPa) and shear displacements of 15 to 18 mm at a shear loading rate of 5 μm/s, and confining pressures of 3 to 6 MPa (see Table 1 for other details).

[19] The topography of the fracture surfaces was measured using the LLNL profilometer [*Durham and Bonner*, 1993] before and after shear in the runs at effective normal

Table 1. Experiment Variables

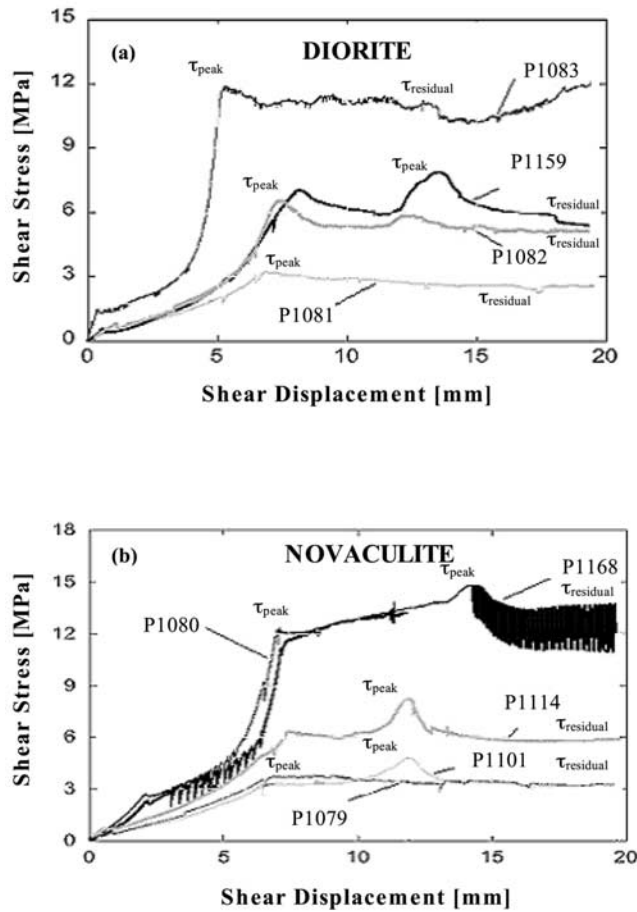| Test	σ_n (MPa)	Pc (MPa)	Pp (MPa)	σ'_n (MPa)	Rock
P1083	20	6	0.1	19.9	diorite
P1159	10	6	0.1	9.9	diorite
P1082	10	6	0.1	9.9	diorite
P1081	5	3	0.1	4.9	diorite
P1168	20	6	0.1	19.9	novaculite
P1080	20	6	0.1	19.9	novaculite
P1114	10	6	0.1	9.9	novaculite
P1101	5	3	0.1	4.9	novaculite
P1079	5	3	0.1	4.9	novaculite

Figure 3. Shear stress as a function of loading shear displacement for (a) diorite and (b) novaculite at a range of effective normal stresses (see Table 1). Note definitions of peak and residual shear stress, which are shown in Figure 4.

stress of 20 MPa. Resolution is ±5 μm perpendicular to the fracture and we sampled at both coarse and fine resolution within the fracture plane. A lateral spacing of 0.1 mm covering an area of 4 × 4 mm (40 × 40 points) comprises the finely resolved profile, with the coarse profile comprising a grid of points spaced at 1 mm over an area of 40 × 40 mm (40 × 40 points).

3. Results

3.1. Mechanical Behavior

[20] The evolution of shear stress as a function of shear displacement is shown in Figure 3. For both samples, shear stress shows an initial rise (before 8 mm) that scales with normal stress and culminates in a peak strength, followed by shear at a residual strength. In the case of diorite (at effective normal stress of 10 MPa) and novaculite (at effective normal stress of 10 and 20 MPa) a third peak is present at large offsets, interpreted as an experimental artifact. The peak shear stress (strength) ranges from 3 to 12 MPa for the diorite and 3 to 15 MPa for the novaculite. In both cases, peak stress and the following residual values are linearly proportional to the applied normal load as shown in Figure 4. Data points in Figure 4 indicate that

experimental reproducibility is quite good, with values of peak and residual strength within ±1 MPa for a given normal stress.

3.2. Hydraulic Behavior

[21] The evolution of permeability as a function of fracture shear displacement is broadly consistent for diorite and novaculite (Figure 5). Two isolated cases exist: one in diorite at an effective normal stress σ of 10 MPa (P1082) and one in novaculite at 20 MPa (P1080). These are outliers are attributed to technical problems in those experiments.

[22] Initial permeability, prior to shear, ranges from 0.5 to 1×10^{-14} m^2, independent of σ and rock type. With shear displacement, fracture permeability drops to a final value equal to 0.5×10^{-17} m^2 recorded at effective normal stresses of 10 and 20 MPa, in diorite; while in novaculite, the final permeability is 1 order of magnitude higher: 0.5×10^{-16} m^2 (at σ of 20 MPa).

[23] We show the relationship between permeability, shear stress, and shear displacement for diorite in Figure 6. These results indicate that at 5 MPa effective normal stresses (Figure 6a) there is little change in permeability with shear. At an effective normal stresses of 10 MPa (Figure 6b) and above (Figure 6c) permeability drops sharply upon reaching the peak strength and then reaches a steady value with continued shear.
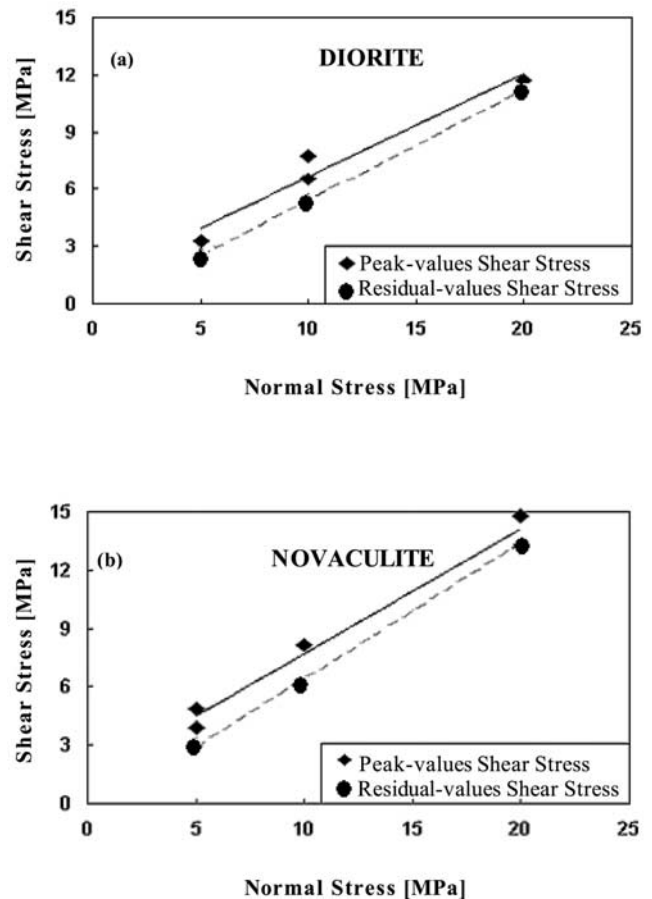

Figure 4. Peak and residual shear stress values as a function of effective normal stress for (a) diorite and (b) novaculite.
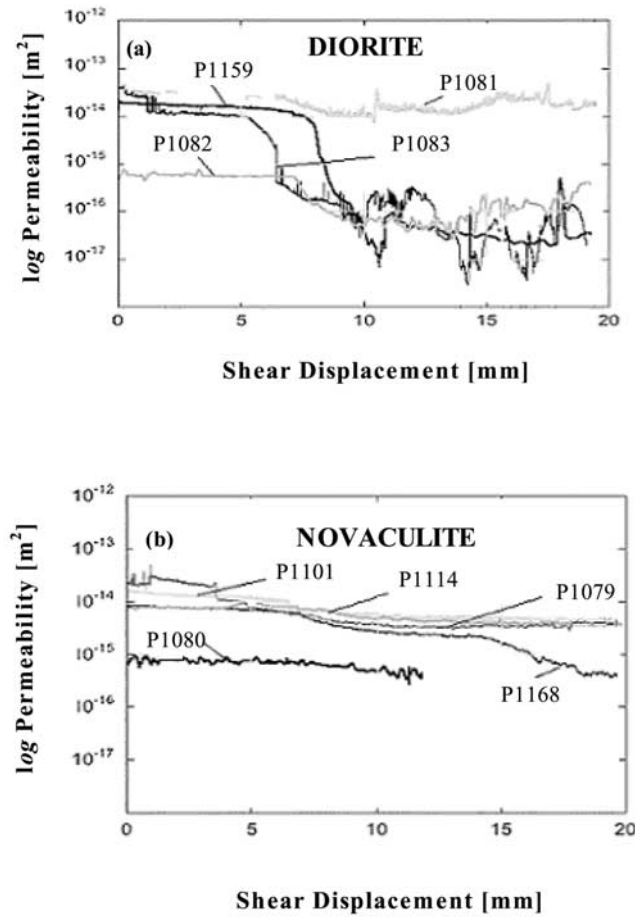
Figure 5. Permeability as a function of shear displacement for (a) diorite and (b) novaculite at a range of effective normal stresses.

3.3. Chemical Behavior

[24] During each test the discharged pore fluid was collected for chemical analysis of the dissolved components; only the elements with the highest aqueous concentrations are reported in Figure 7. Of the measured components, only magnesium concentrations are highest and are the only components to vary appreciably with the applied effective normal stress. However, Mg is a contaminant in the pore fluid from the testing equipment and is not considered further here. Aqueous concentrations of the other components increase slightly with shear displacement during the experiments on diorite (K) and show a larger increase with displacement for novaculite (Si).

4. Discussion and Conclusions

[25] Our experiments were designed to determine the evolution of strength and permeability of artificial, relatively smooth fractures in diorite and novaculite. We find that shear stress evolves with shear displacement, with steady state values reached after ~10 mm (diorite) and ~15 mm (novaculite) of load point displacement. En route to the peak strength, multiple peaks in shear stress are observed in some cases. The first systematic peak usually occurs before 2 mm and is attributed to stretching of the sample-encasing

rubber membrane. The remaining peaks are interpreted as functions of the asperity distribution of the contact surfaces.

[26] Although all the samples were roughened in the same manner using #60 grit polishing compound, the resulting surfaces in novaculite appeared smoother than those in diorite (Figures 8–10). The profiles for the samples are shown pretest and posttest (Figures 8–10) and these show changes in the short wavelength roughness as a result of shearing. The pretest images of roughness show sharp peaks in the asperity distribution; and these are removed as a result of shearing. At coarser resolution, the posttest distributions for diorite show longer wavelength features of the roughness spectrum (Figure 10).

[27] The images of surface roughness provide important information for understanding the evolution of friction with shear (Figure 11). For diorite, the stress displacement curves indicate that asperities are sufficiently smooth that fracture slip occurs without long-term slip hardening (Figure 3). On
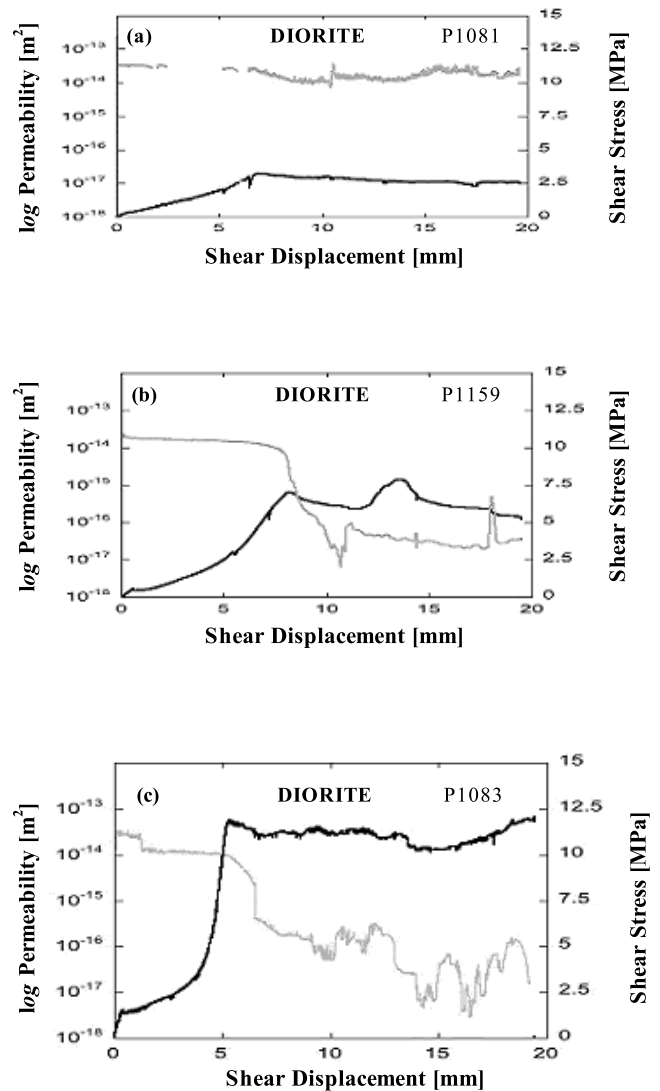

Figure 6. Plots showing the relationship between permeability, shear stress, and shear displacement for diorite at effective normal stresses of (a) 5 MPa, (b) 10 MPa, and (c) 20 MPa.
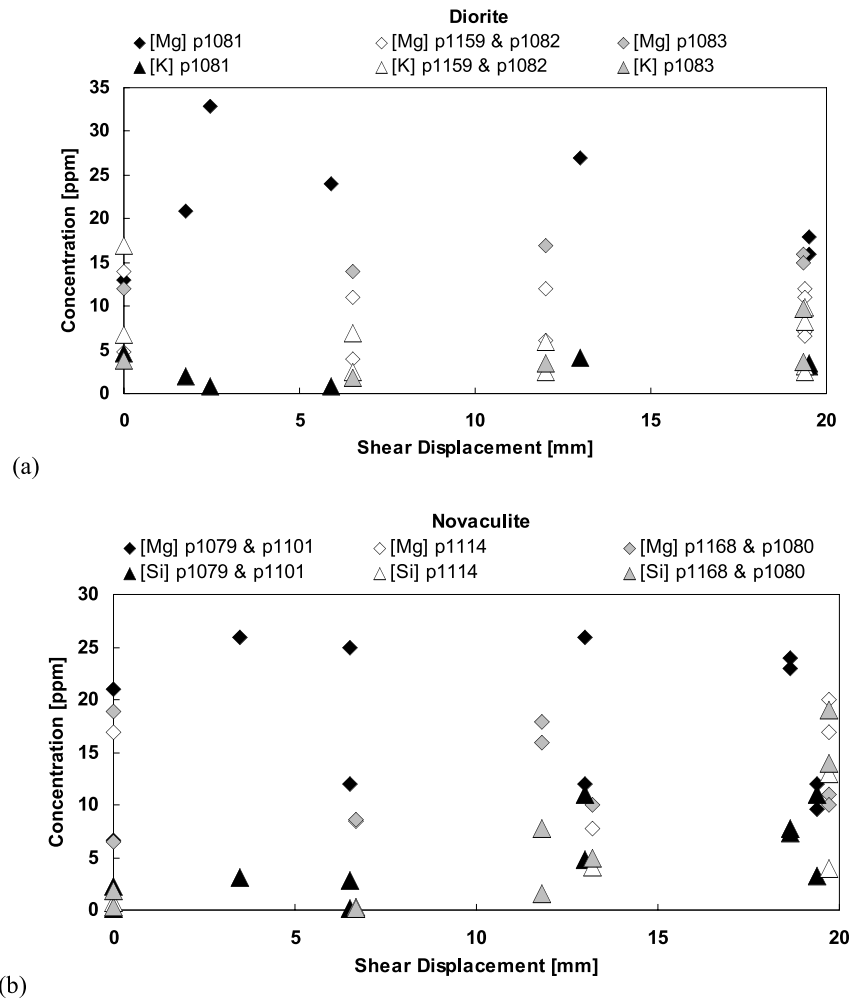
Figure 7. Concentration of major ions in the pore fluid as a function of net shear displacement for (a) diorite and (b) novaculite at a range of effective normal stresses (Table 1).
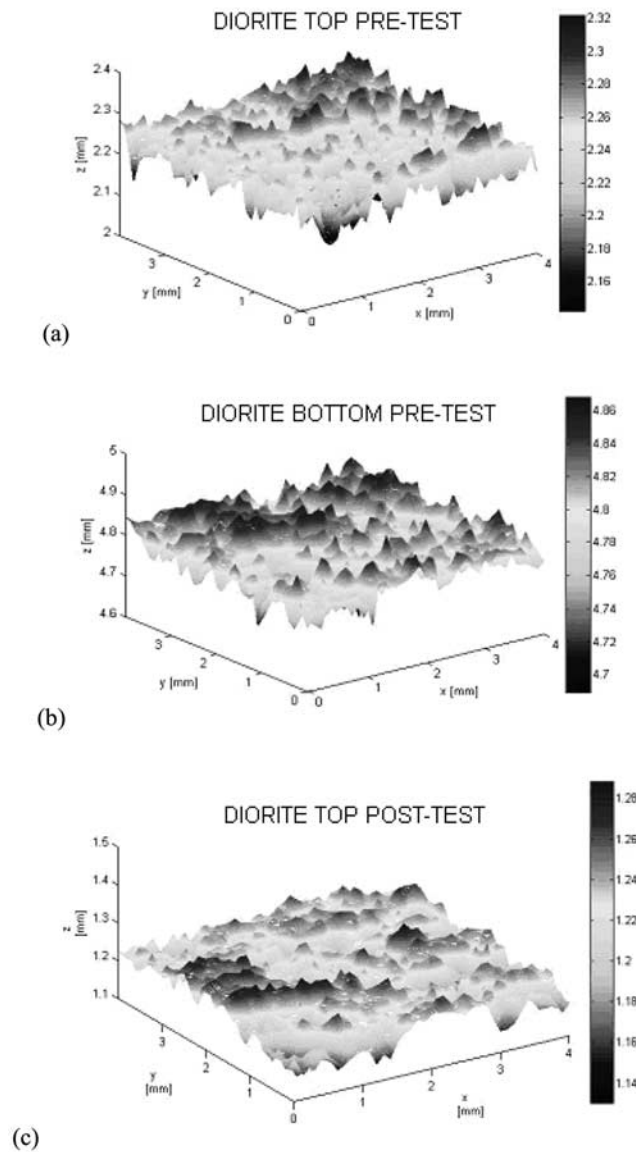
(a)

(b)

(c)

Figure 8. Surface roughness images determined from probe profilometer. Relative range (x, y, z) is the same for each image. (a) Pretest surface of the large (45 × 70 mm) diorite block (see Figure 2). (b) Pretest surface of the smaller (45 × 50 mm) diorite block. (c) Posttest surface of the large (45 × 70 mm) diorite block; same surface as in Figure 8a.

[28] Results show that both in diorite and in novaculite the initial values of fracture permeability range between 0.5 and 1.0×10^{-14} m^2, independent of the effective normal stresses. This equates to equivalent hydraulic apertures in the range $15-20$ μm (see Figure 12). Upon shearing the permeability drops to the final steady value of 0.5×10^{-17} m^2 recorded at effective stresses of 10 and 20 MPa and corresponds to an equivalent hydraulic aperture to 2 μm in diorite. Novaculite behaves similarly but the final permeability is 0.5×10^{-16} m^2 and it is obtained only at an effective normal stress of 20 MPa.

[29] The evolution of permeability during shear is clearly related to surface roughness and the development of wear products. Magnitudes of preshear permeability are only weakly related to the roughness of the contacting surfaces, evidenced since all surfaces return similar magnitudes of initial permeability, and these are insensitive to normal stress. Although the shear resistance is influenced by roughness, with multiple peaks in shear resistance ascribed to the characteristics of the roughness profile, this influence has little impact on postpeak permeabilities. This observation is consistent with the production of wear products during shear.
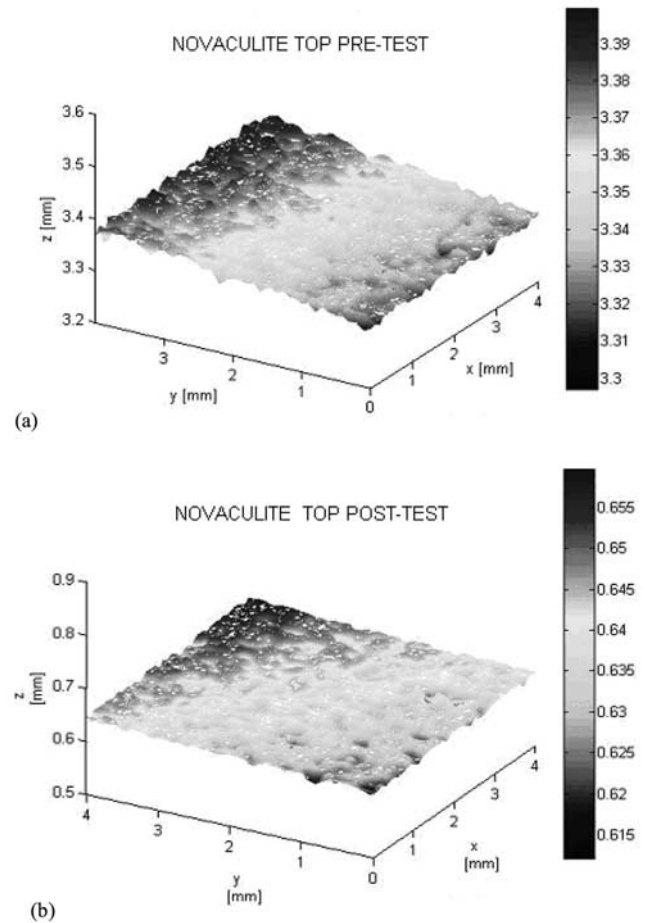

(a)

(b)

Figure 9. Surface roughness images determined from probe profilometer. Relative range (x, y, z) is the same for each image. (a) Pretest surface of the small (45 × 50 mm) novaculite block (see Figure 2). (b) Posttest surface of the smaller (45 × 50 mm) novaculite block.

the contrary, for novaculite, we see a prominent second peak strength between 10 and 15 mm of slip. This suggests that the asperity height distribution is broad, with few or no prominent features. Figure 11 shows the coefficient of friction μ (ratio between shear and effective normal stresses) as a function of the shear displacement. For both rock types, the residual friction value ranges between 0.6 and 0.7 and this is justifiable considering the final evolution of the smooth surface in the samples. These data are consistent with expectations for friction between two flat plates, which is principally related to the roughness of the surfaces rather than their composition.
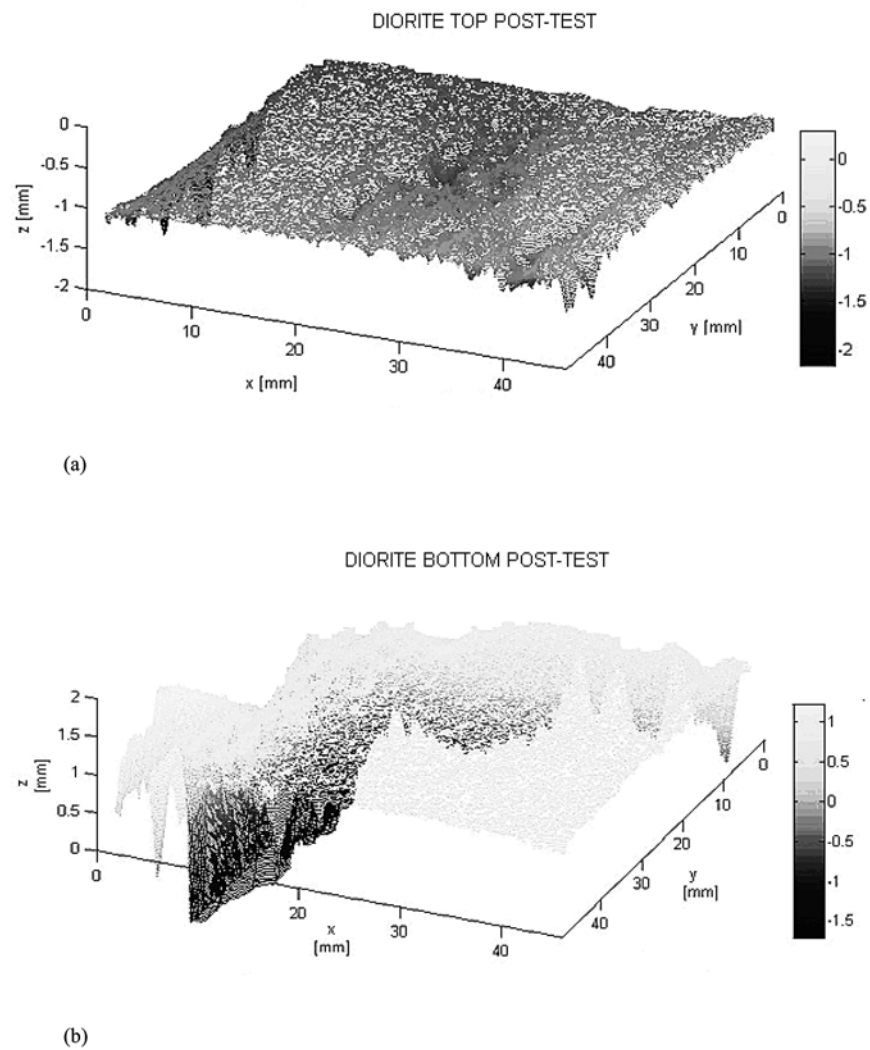
(a)

(b)

Figure 10. Surface roughness images determined from probe profilometer. These are coarser (x, y) views of the images shown in Figure 9. (a) Posttest surface of the small (45 × 50 mm) diorite block. (b) Posttest view of the larger (45 × 70 mm) diorite block.
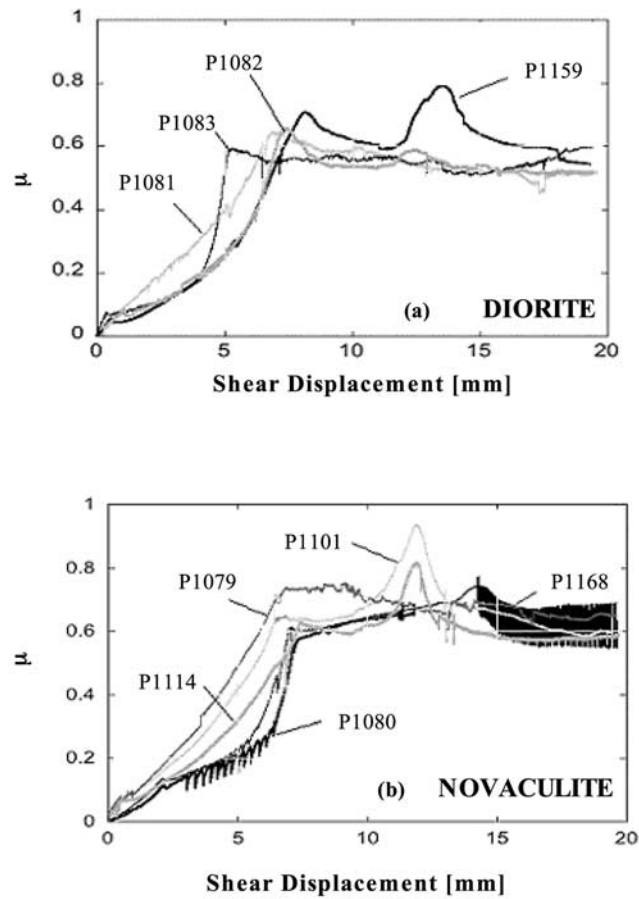
Figure 11. Friction coefficient as a function of shear displacement for (a) diorite and (b) novaculite at each effective normal stress.

[30] In the case of diorite, in which the initial surfaces are rougher than for the novaculite, the production of gouge occurs more readily. Significant gouge is produced, as evidenced by the permeability response, at earlier shear offsets (at 6 mm offset in diorite compared with at 17 mm in novaculite at 20 MPa), and at lower stresses (already at 10 MPa for diorite). The observation that the permeability in diorite is the same at effective stresses of either 10 or 20 MPa can be explained by considering that the wear rate is approximately constant, independent of normal stress in this range. Finally, the difference in the large-offset permeabilities observed at all stresses in diorite and novaculite are attributed to the relatively larger production of wear products in the higher-amplitude roughness of the diorite. As expected, where mean permeabilities are converted to equivalent hydraulic apertures (Figure 12), the apertures mirror the consistency between permeabilities recovered in a single rock type but at multiple stresses, and emphasize the difference between rock types. Although reducing data to an equivalent hydraulic aperture is inappropriate where permeability is controlled by wear products, the evolution of preshear apertures from between 15 and 20 μm to final values of 2–4 μm (diorite) and 5 μm (novaculite) is consistent with a model implicating wear products.

[31] Observed aqueous concentrations at outlet increase slightly with shear offset in the experiments, on diorite and increase more markedly for the experiments on novaculite. This increase is attributed to the corresponding anticipated generation of wear products. Except for the presence of magnesium (implicated as a residue in the fluid capture system from prior experiments), all components increase in concentration with both shear offset and the corresponding duration of the test (Figure 7). These twin effects of shear offset and residence time can be separated by noting that multiple void volumes flush the sample in a single experiment. Thus the observed increase in concentration with time is linked most strongly to the evolution of increased surface area from the development of comminution products. These concentrations and related rates of dissolution are rapid in a geologic sense, and are sufficiently rapid to have influence in engineering timeframes.

[32] These experiments are reported with rigorous control on stress and fluid transport conditions, but with relatively less control on the evolution of surface topography and the effects of wear. Regardless, the role of wear products in mediating changes in permeability with offset, is largely independent of initial conditions of surface roughness, and especially insensitive to magnitudes of normal stress level. Correspondingly, inferences in the evolution of permeability may be linked to initial magnitudes of surface roughness and in the corresponding potential to generate wear products, in part related to the granular or crystalline nature of the rock type.
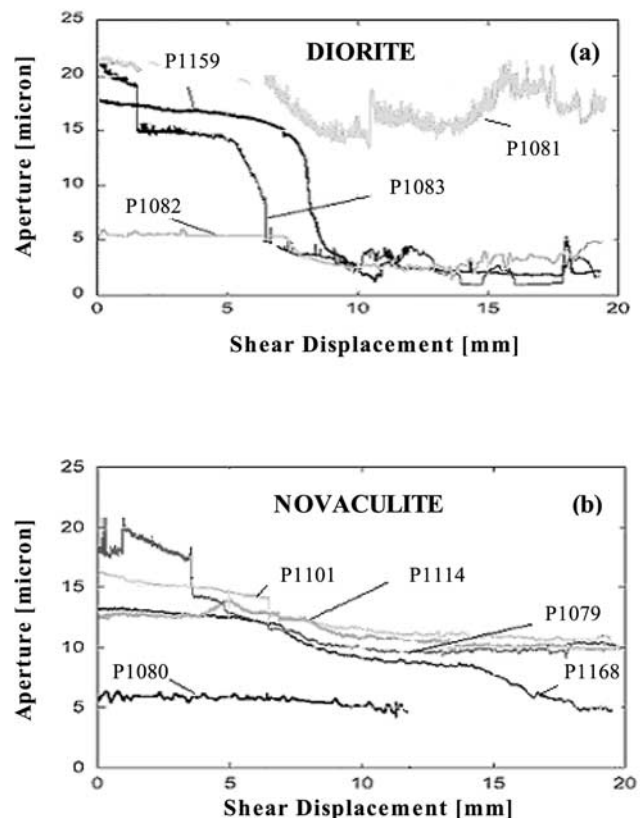

Figure 12. Hydraulic aperture determined from hydraulic conductivity, assuming the cubic law for fracture flow, as a function of shear displacement for (a) diorite and (b) novaculite at each effective normal stress.

References

Bayuk, I. O., and E. M. Chesnokov (1998), Correlation between elastic and transport properties of porous cracked anisotropic media, *Phys. Chem. Earth*, 23, 361–366, doi:10.1016/S0079-1946(98)00038-X.

Cook, N. G. W. (1992), Natural joints in rocks: Mechanical, hydraulic and seismic behaviour and properties under normal stress, *Int. J. Rock Mech. Min. Sci. Geomech. Abstr.*, 29, 198–223, doi:10.1016/0148-9062(92)93656-5.

Crampin, S., and S. Chastin (2003), A review of shear wave splitting in the crack-critical crust, *Geophys. J. Int.*, 155, 221–240, doi:10.1046/j.1365-246X.2003.02037.x.

Durham, W. B., and B. P. Bonner (1993), PEAK: A new kind of surface microscope, *Int. J. Rock Mech. Min. Sci. Geomech. Abstr.*, 30, 699–702, doi:10.1016/0148-9062(93)90008-2.

Durham, W. B., W. L. Bourcier, and E. A. Burton (2001), Direct observation of reactive flow in a single fracture, *Water Resour. Res.*, 37(1), 1–12, doi:10.1029/2000WR900228.

Elias, B. P., and A. Hajash (1992), Change in quartz solubility and porosity change due to effective stress: An experimental investigation of pressure solution, *Geology*, 20, 451–454, doi:10.1130/0091-7613(1992)020<0451:CIQSAP>2.3.CO;2.

Elkibbi, M., and J. A. Rial (2003), Shear wave splitting: An efficient tool to detect 3D fracture patterns at the Geysers, California, paper presented at 28th Workshop on Geothermal Reservoir Engineering, Stanford Univ., Stanford, Calif.

Elkibbi, M., and J. A. Rial (2005), The Geysers geothermal field: Results from shear-wave splitting analysis in a fractured reservoir, *Geophys. J. Int.*, 162, 1024–1035, doi:10.1111/j.1365-246X.2005.02698.x.

Gratier, J. P. (1993), Experimental pressure solution of halite by an indenter technique, *Geophys. Res. Lett.*, 20, 1647–1650, doi:10.1029/93GL01398.

Hajash, A., T. D. Carpenter, and T. A. Dewers (1998), Dissolution and time-dependent compaction of albite sand: Experiments at 100°C and 160°C in pH-buffered organic acids and distilled water, *Tectonophysics*, 295, 93–115, doi:10.1016/S0040-1951(98)00117-6.

King, M. S. (2002), Elastic wave propagation in and permeability for rocks with sets of aligned fractures, in *Proceedings of the 5th International Workshop on the Application of Geophysics to Rock Engineering*, edited by R. P. Young, pp. 14–19, Int. Soc. for Rock Mech., Lisbon, Portugal.

Lin, W., and W. Daily (1990), Hydrological properties of Topopah Spring tuff under a thermal gradient—Laboratory results, *Int. J. Rock Mech. Min. Sci. Geomech. Abstr.*, 27(5), 373–386, doi:10.1016/0148-9062(90)92712-N.

Lin, W., J. Roberts, W. Glassley, and D. Ruddle (1997), Fracture and matrix permeability at elevated temperatures, paper presented at Workshop on Significant Issues and Available Data, Near-Field/Altered-Zone Coupled Effects Expert Elicitation Project, San Francisco, Calif., 5–7 Nov.

Liu, E., X.-Y. Li, and J. H. Queen (2001), Discrimination of pore fluids from P and converted shear-wave AVO analysis, in *Anisotropy 2000: Fractures, Converted Waves and Case Studies, Proceedings of the Ninth International Workshop on Seismic Anisotropy*, edited by L. Ikelle and A. Gangi, pp. 203–221, Soc. of Explor. Geophys., Tulsa, Okla.

Liu, E., S. R. Tod, and X.-Y. Li (2002), Effects of stress and pore fluid pressure on seismic anisotropy in cracked rocks, *Canadian SEG*, 27, 92–98.

Liu, E., S. Vlastos, X.-Y. Li, I. G. Main, and M. Schoenberg (2004), Modeling seismic wave propagation during fluid injection in a fractured network: Effects of pore fluid pressure on time-lapse seismic signatures, *Lead. Edge*, 23, 778–783, doi:10.1190/1.1786902.

Lou, M., and J. A. Rial (1997), Characterization of geothermal reservoir crack patterns using shear-wave splitting, *Geophysics*, 62, 487–495, doi:10.1190/1.1444159.

Maultzsch, S., M. Chapman, E. Liu, and X. Y. Li (2003), Modelling frequency-dependent seismic anisotropy in fluid-saturated rock with aligned fractures: Implication of fracture size estimation from anisotropic measurements, *Geophys. Prospect.*, 51, 381–392, doi:10.1046/j.1365-2478.2003.00386.x.

Moore, D. E., D. A. Lockner, and J. D. Byerlee (1994), Reduction of permeability in granite at elevated temperatures, *Science*, 265, 1558–1561, doi:10.1126/science.265.5178.1558.

Polak, A., D. Elsworth, H. Yasuhara, A. S. Grader, and P. M. Halleck (2003), Permeability reduction of a natural fracture under net dissolution by hydrothermal fluids, *Geophys. Res. Lett.*, 30(20), 2020, doi:10.1029/2003GL017575.

Pyrak-Nolte, L. J. (2002), Seismic imaging of fractured media, *Proc. 5th Int. Workshop on Appl. Geophys. in Rock Eng.*, Toronto, Ont., 5–13.

Raj, R. (1982), Creep in polycrystalline aggregates by matter transport though a liquid phase, *J. Geophys. Res.*, 87, 4731–4739, doi:10.1029/JB087iB06p04731.

Rasolofosaon, H., and I. Zinszner (2002), Comparison between permeability anisotropy and elastic anisotropy of reservoir rock, *Geophysics*, 67, 230–240, doi:10.1190/1.1451647.

Sahimi, M. (1993), Flow phenomena in rocks: From continuum models to fractals, percolation, cellular automata and simulated annealing, *Rev. Mod. Phys*, 65, 1393–1534, doi:10.1103/RevModPhys.65.1393.

Sahimi, M. (1995), *Flow and Transport in Porous Media and Fractured Rock*, VCH, Weinheim, Germany.

Siddiqi, G., B. Evans, G. Dresen, and D. Freund (1997), Effect of semi-brittle deformation on transport properties of calcite rocks, *J. Geophys. Res.*, 102, 14,765–14,778, doi:10.1029/97JB01038.

Tada, R., and R. Siever (1989), Pressure solution during diagenesis, *Annu. Rev. Earth Planet. Sci.*, 17, 89–118, doi:10.1146/annurev.ea.17.050189.000513.

Tadokoro, K., and M. Ando (2002), Evidence for rapid fault healing derived from temporal changes in *S* wave splitting, *Geophys. Res. Lett.*, 29(4), 1047, doi:10.1029/2001GL013644.

Tenthorey, E., S. F. Cox, and H. F. Todd (2003), Evolution of strength recovery and permeability during fluid-rock reaction in experimental fault zones, *Earth Planet. Sci. Lett.*, 206, 161–172, doi:10.1016/S0012-821X(02)01082-8.

Vlahovic, G., M. Elkibbi, and J. A. Rial (2003a), Shear-wave splitting and reservoir crack characterization: The Coso geothermal field, *J. Volcanol. Geotherm. Res.*, 120, 123–140, doi:10.1016/S0377-0273(02)00368-2.

Vlahovic, G., M. Elkibbi, and J. A. Rial (2003b), Temporal variations of fracture directions and fracture densities in the Coso geothermal field from analyses of shear-wave splitting, paper presented at 27th Workshop on Geothermal Reservoir Engineering, Stanford Univ., Stanford, Calif.

Yang, M., M. Elkibbi, and J. A. Rial (2005), An inversion scheme to model subsurface fracture systems using shear wave splitting polarization and delay time observations simultaneously, *Geophys. J. Int.*, 160, 939–947, doi:10.1111/j.1365-246X.2005.02532.x.

Yasuhara, H., D. Elsworth, and A. Polak (2004), Evolution of permeability in a natural fracture: Significant role of pressure solution, *J. Geophys. Res.*, 109, B03204, doi:10.1029/2003JB002663.

Yasuhara, H., C. Marone, and D. Elsworth (2005), Fault zone restrengthening and frictional healing: The role of pressure solution, *J. Geophys. Res.*, 110, B06310, doi:10.1029/2004JB003327.

Zhang, S., S. Cox, and M. Paterson (1994), The influence of room temperature deformation on porosity and permeability in calcite aggregates, *J. Geophys. Res.*, 99, 761–775.

————————————
D. Elsworth, I. Faoro, and A. Niemeijer, Department of Energy and Mineral Engineering, Pennsylvania State University, University Park, PA 16802, USA. (iufl03@psu.edu)

C. Marone, Department of Geosciences, Pennsylvania State University, University Park, PA 16802, USA.